CCFE
CULHAM CENTRE FOR FUSION ENERGY

UK Atomic Energy Authority

UKAEA-CCFE-PR(19)36

Y. Q. Wang, S. J. Clark, B. Cai, D. Alba Venero, K. Yan, M. Gorley, E. Surrey, D. G. McCartney, S. Sridhar, P. D. Lee

Small-angle neutron scattering reveals the effect of Mo on interphase nano-precipitation in Ti-Mo micro-alloyed steels

Small-angle neutron scattering reveals the effect of Mo on interphase nano-precipitation in Ti-Mo micro-alloyed steels

Y. Q. Wang, S. J. Clark, B. Cai, D. Alba Venero, K. Yan, M. Gorley, E. Surrey, D. G. McCartney, S. Sridhar, P. D. Lee

This is a preprint of a paper submitted for publication in Scripta materialia

Small-angle neutron scattering reveals the effect of Mo on interphase nano-precipitation in Ti-Mo micro-alloyed steels

Y. Q. Wang[a*, b], S. J. Clark[b, c], B. Cai[d], D. Alba Venero[e], K. Yan[f], M. Gorley[a], E. Surrey[a], D. G. McCartney[b, g], S. Sridhar[h], P. D. Lee[b, c*]

[a] *United Kingdom Atomic Energy Authority, Culham Science Centre, Abingdon, OX14 3DB, UK*
[b] *Research Complex at Harwell, Rutherford Appleton Laboratory, Harwell, OX11 0FA, Oxfordshire, UK*
[c] *Department of Mechanical Engineering, University College London, Torrington Place, London WC1E 7JE, UK*
[d] *School of Metallurgy and Materials, University of Birmingham, Birmingham, UK*
[e] *ISIS, STFC Rutherford Appleton Laboratory, Didcot, Oxfordshire, OX11 0QX, UK*
[f] *School of Materials, University of Manchester, Manchester, M13 9PL, UK*
[g] *Advanced Materials Group, University of Nottingham, Nottingham, NG7 2RD, UK*
[h] *George S. Ansell Department of Metallurgical and Materials Engineering, Colorado School of Mines, Golden, CO 80401, USA*

[*] Corresponding authors: Yiqiang Wang (yiqiang.wang@ukaea.uk)

Abstract

Ti-containing micro-alloyed steels are often alloyed with molybdenum (Mo) to gain superior ageing-resistance through reduced nano-precipitate coarsening, although the exact mechanism is still disputed. Using small angle neutron scattering (SANS), we characterize precipitate composition and coarsening in Ti micro-alloyed steels with and without Mo through analysis of both the nuclear and magnetic signals. The SANS results are correlated to phase transformations, precipitation formation and mechanical properties of the steels. The SANS results demonstrate that~25 at.% of Ti is substituted by Mo in the (Ti, Mo)C precipitates, increasing both the precipitate volume percent (from ~0.1% to ~0.13%) and average size at a given ageing time. Our study reveals that Mo does not play a role in retarding coarsening of the precipitates, which is contrary to existing literature. The mechanism providing Ti-Mo steels with improved ageing-resistance is believed due to the improved misfit between precipitate and matrix, delaying loss of coherency. This new understanding opens opportunities for design of ageing-resistant microalloyed steels with use of significantly less amount of costly Mo.

Keywords: Micro-alloyed steel, Interphase Precipitation, Small-Angle-Scattering.

High-strength low-alloy steels strengthened through the interphase precipitation (IPP) mechanism have seen a revival for automotive industry since the development of the NANOHITEN steel which has tensile strengthen up to 780 MPa [1]. IPP is the phenomenon that occurs upon the decomposition of austenite in steels containing strong carbide -forming elements (such as Ti, Mo and V) and results in characteristic periodic planes of fine precipitates [2, 3]. In low-carbon steel fine MC (M = Ti, Mo or V) IPP are encapsulated within a soft ferritic matrix which is strengthened through the Orowan mechanism [4] yielding a steel with high strength and formability [5].

However, these MC particles can coarsen during hot rolling or subsequent annealing heat treatment, degrading the strength of the materials significantly. One possible solution reported in the literature is the addition of molybdenum (Mo). Funakawa and Seto [6], and later work conducted by others [7-10] found that steels with Mo additions showed mechanical properties were retained longer during high-temperature ageing. These studies were compared to the observed interphase precipitation in Ti-containing (~0.2wt%) and Ti-Mo-containing (~0.1wt%Ti and ~0.2wt%Mo) low carbon steels with a fixed basic composition ~0.04%C, 1.5%Mn, 0.2%Si in wt.%. It can be seen that in these studies, the atomic ratio of Ti:C and (Ti+Mo):C were designed to be ~1:1. The most well-known mechanism for this effect was reported by Jang et al. [8], who used first principles calculations to propose that the Mo only participates during the early stages of precipitation and becomes passive due to the energetic disadvantage during the subsequent growth and coarsening stages. The coarsening of precipitates is mainly controlled by diffusion of Ti atoms, therefore, the replacement of Ti by Mo reduces the Ti concentration in the ferrite matrix, which decelerates the coarsening of (Ti, Mo)C precipitates [6, 8]. Moreover, Funakawa *et al.* [6] observed that a decrease in Ti concentration from 0.2wt% to ~0.1wt% without Mo additions in Ti-containing steel results in similar hardness of Ti-Mo-containing one (~0.1wt%Ti and ~0.2wt%Mo). Jang *et al.*, [11] used CALPHAD and diffusion simulations to show that the coarsening rate of TiC in Fe-Ti-C steels (fixed 0.04%C, wt%) can be significantly retarded by decreasing the Ti/C ratio.

However, both the effect of Ti/C ratio and the Mo on the interphase precipitation have not been well examined quantitatively, which leaves a question to the automotive industry whether it is necessary to add Mo into Ti-containing steels. This is due to the widely used techniques such as transmission electron microscopy (TEM) [12, 13] and atom probe tomography (APT) [14-18] which have a limited capability to analyse statistically significant numbers of precipitates. The size difference of precipiates between Ti and Ti-Mo alloys presented in the literature is so small (typically in the range of 1.6 nm to 10 nm [7-9]) that it is difficult to statistically and accurately investigate the the role of Mo with TEM and APT.

The present study utilizes bulk characterization, via Small-Angle-Neutron-Scattering (SANS), of two micro-alloyed steels aged at 650°C for various times. One alloy (Fe-0.79Ti-0.051C-1.63Mn-0.19Si-0.036Al-0,014P-0.006S-0.007N, wt%) contains Ti with a Ti:C atomic ratio of 0.4. The second alloy (Fe-0.7Ti-0.2Mo-0.044C-1.58Mn-0.19Si-0.039Al-0,013P-0.005S-

0.0046N, wt%) contains Ti and Mo with a (Ti+Mo):C atomic ratio of ~1. The detailed characterization was undertaken using SANS, through analysis of both the nuclear and magnetic signals, giving quantitative insight into the evolution of the average precipitate size, volume percent, and precipitate chemistry in bulk samples, which are key informaiton to uncover the precipitation kinetics and hardening behaviour.

The alloys were vacuum induction melted, casted and then forged at about 1250 °C followed by air cooling. Pieces 30×10×5 mm^3 were sectioned and heat treated (See Supplementary Fig. S1a). Firstly, the specimens were austenitized in a salt bath at 1250 °C for 300 s to dissolve pre-existing precipitates and water quenched. Secondly, the specimens were austenitized at 950 °C for 120 s (to control the austenite grain size) then transferred directly to a salt bath at 650 °C for periods ranging from 0 to 36 ks and water quenched. Prolonged long-term ageing for a further 144 ks was performed separately.

SANS experiments were performed on the SANS2d beamline at the ISIS Pulsed Neutron Source, UK [19]. A magnetic field of 1.5 T was applied to saturating the ferritic matrix which allows to separate the magnetic and nuclear scattering. Specimens with dimension of ~9 mm×~9 mm× ~1 mm were cut from the heat treated samples for the SANS measurements. The neutron beam size was 8mm in diameter and the measurement time was set to 60min. The sample to detector distance was 4m which gave scattering vector, *q*, covered the range of 0.004 to 0.3 $Å^{-1}$. To avoid collecting scattering signal from multi-Bragg diffraction, only neutrons with wavelengths, λ, from 4.5 to 16.5 Å were selected for data analysis [20]. One-dimensional nuclear and "nuclear + magnetic" scattering intensity plots, *I* (intensity) versus *q* were obtained by partial azimuthal averaging in 30 sectors around the horizontal and vertical axes of the transmitted beam respectively using the software Mantidplot [21].

The microstructures of polished and 2% Nital etched samples were examined using scanning electron microscopy (SEM) via an FEI Quanta 650 FEG-SEM operated at a voltage of 20 kV. Detailed microstructures of the (Ti,Mo)C precipitates were examined using a JEOL 2100 TEM. Thin foil specimens were mechanically polished to ≈30 μm in thickness followed by ion beam milling to electron transparency. The microhardness (Hv) of ferrite grains in heat treated samples was measured using a microhardness tester with a load of 0.1 kgf. 20 measurements were conducted for each sample.

Fig.1a shows the mean value of Hv versus age time at 650 °C for both Ti and Ti-Mo containing steels and the error-bar represents one standard deviation. The Ti-Mo containing steels show slightly higher hardness and better ageing-resistance compared to the steel with only Ti additions. As shown in Figs. 1b and 1c, the γ to α transformation in both alloys occurs rapidly and both reached ~90% completion in a similar duration of 60 s. This agrees with the dilatometry results (Supplementary Fig. S1b). Figs. 1b, 1c, 1d and 1e also show that decreasingly small regions of bainite formed during quenching with increasing isothermal holding. Both SEM and dilatometry measurements reveal that Mo has a small effect on the γ to α transformation. Bright field TEM images of the Ti and Ti-Mo containing samples

transformed at 650°C for 36 ks are shown in Figs. 2(e) and (f). In both alloys, characteristic periodic planes of nanoscale precipitates are observed, indicative of interphase precipitation.

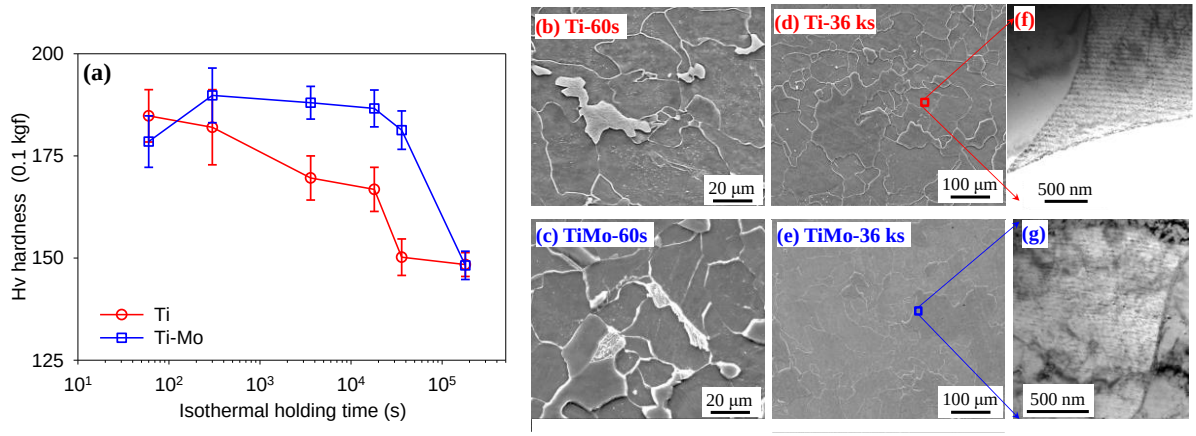

Fig. 1. (a) Effect of isothermal holding time, t, on measured microhardness, Hv, of the Ti and Ti-Mo steels held at 650 °C. Error bars in Hv correspond to one standard deviation from the mean. (b) to (e) SEM images of the Ti (b and c) and TiMo (d and e) samples isothermally transformed for 60 s and 36 ks. (f) and (g) Bright field TEM images of the Ti and TiMo steels respectively after ageing for 36 ks showing interphase precipitation.

Fig. 2 shows the one dimensional nuclear and magnetic SANS data in the form of Iq^2 versus scattering vector (q) (left hand axis) for the selected isothermally transformed (60 s, 36 ks and 180 ks) alloys. The results for the water quenched sample and the remaining isothermally transformed (0.3ks, 3.6 ks and 18 ks) samples are shown in Supplementary Figs. S2 and S3. The ratio of magnetic scattering ($I_{mag}(q)$) to nuclear scattering ($I_{nuc}(q)$) intensity, $R(q)$, which is related to the precipitate composition, is shown on the left-hand axis. If all precipitates have the same composition then the value of $R(q)$ would be constant. On the other hand, $R(q)$ would vary if there were more than one type of precipitate present of differing size [22]. Cleary, there were two types of particles with significant difference in both size and composition formed in both steels revealed by two different $R(q)$ values of ~3 and ~1 at low (0.004 to ~0.01 Å^{-1}) and high (0.02 to ~0.1 Å^{-1}) q region respectively.

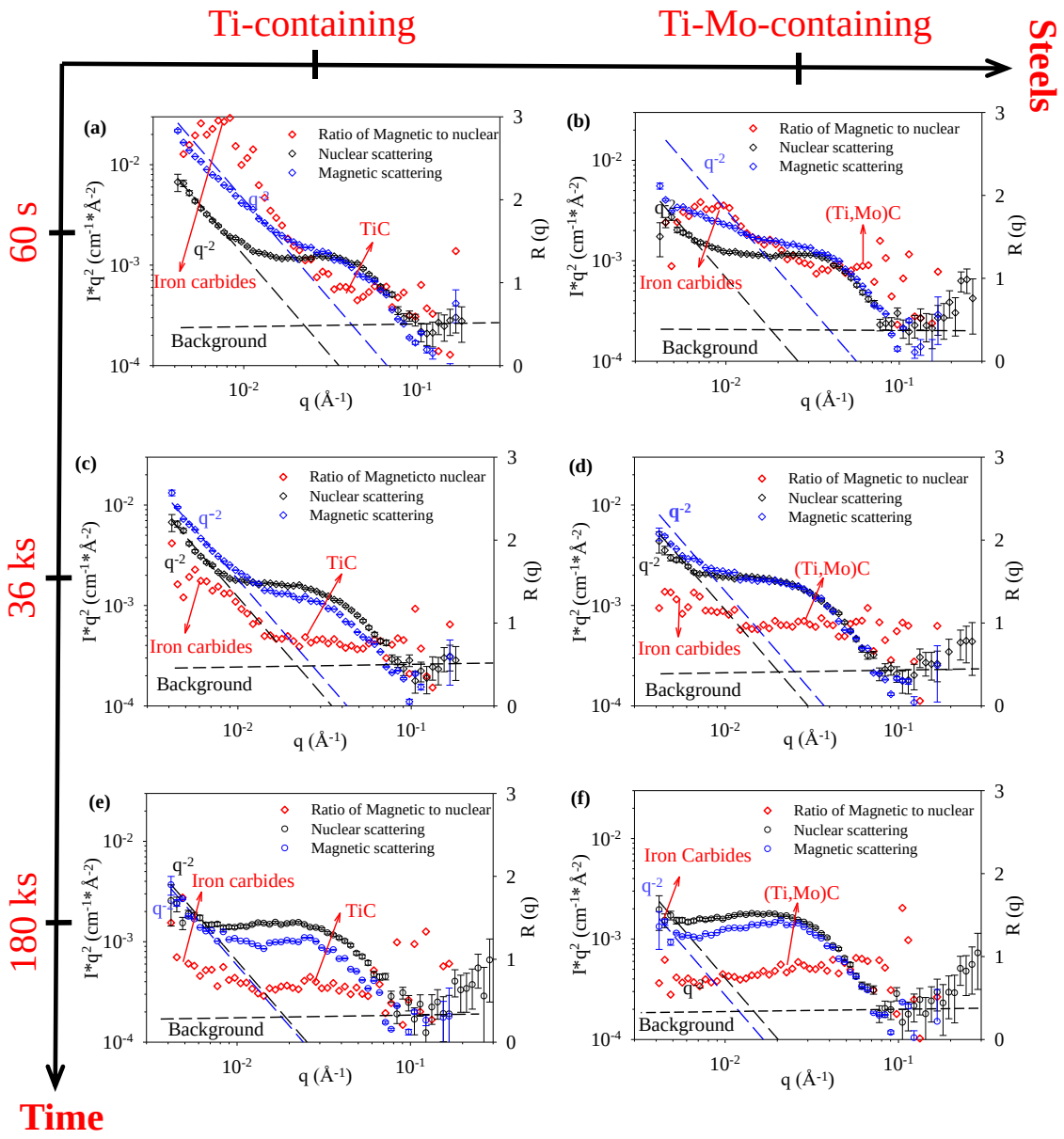

Fig. 2. One-dimensional nuclear and magnetic SANS patterns of Iq^2 (left hand axis) and R(q) (right hand) axis versus scattering vector, q, obtained from the (a, c and e) Ti and (b, d, and f) TiMo samples isothermally transformed at 650 °C for (a and b) 60 s, (c and f) 36 ks, (e and f) 180 ks180 ks respectively.

In the low q region, $R(q)$ increases due to the presence of large iron carbides and this is seen to exist in the Ti-containing steels up to 180 ks. In the Ti-Mo containing steels, there is less evidence for an increase in $R(q)$ at low q suggesting less iron carbide forms in this steel. The scattering from large scale iron carbides also reveals itself in the form of a Porod Law slope of approximately q^{-2} on the plot of Iq^2 versus q at the low q region. These large iron carbides (Figs. 1b and 1c), make only a small contribution to the nuclear scattering signal but a significant contribution to the magnetic scattering signal. This causes to a marked difference between these two signals at low q as revealed by an increase in the $R(q)$ value. In the samples isothermally held for 180 ks, the matrix phase transformation was completed so

iron carbides did not form following quenching resulting in a smaller difference between the nuclear and magnetic signals across the entire range of q. At high q region, it is the fine IPP that contribute to the nuclear and magnetic signals and so $R(q)$ plateaus from which the chemical composition of the IPP can be estimated.

To isolate the scattering signal only from nano-sized TiC or (Ti, Mo)C precipitates the Porod Law region at low q and the incoherent background in both the nuclear and magnetic SANS signals were subtracted. Fig. 3 shows the mean values of $R(q)$, which were calculated by taking the average of $R(q)$ values in the q range from ~0.0194 to ~0.0775 $Å^{-1}$ (for samples aged for 60s to 3.6 ks) and ~0.0097 to ~0.0664 $Å^{-1}$ (for samples aged from 18 ks to 180 ks). The error in Fig. 3 is given as one standard deviation. The results show that the mean values of $R(q)$ for isothermally transformed Ti and Ti-Mo alloys were ~0.75 and ~1 respectively. The ageing time did not change the mean values of $R(q)$ significantly. The theoretical $R(q)$ values of ~0.75 and ~1 represent the average chemical composition of the precipitates in Ti and Ti-Mo containing steels are TiC and $Ti_{0.75}Mo_{0.25}C$ respectively [21], as shown by the red and blue horizontal lines in Fig. 3. This is in reasonable agreement with the 3D APT data obtained by Mukherjee *et al.* [23] and Wang et al. [18].

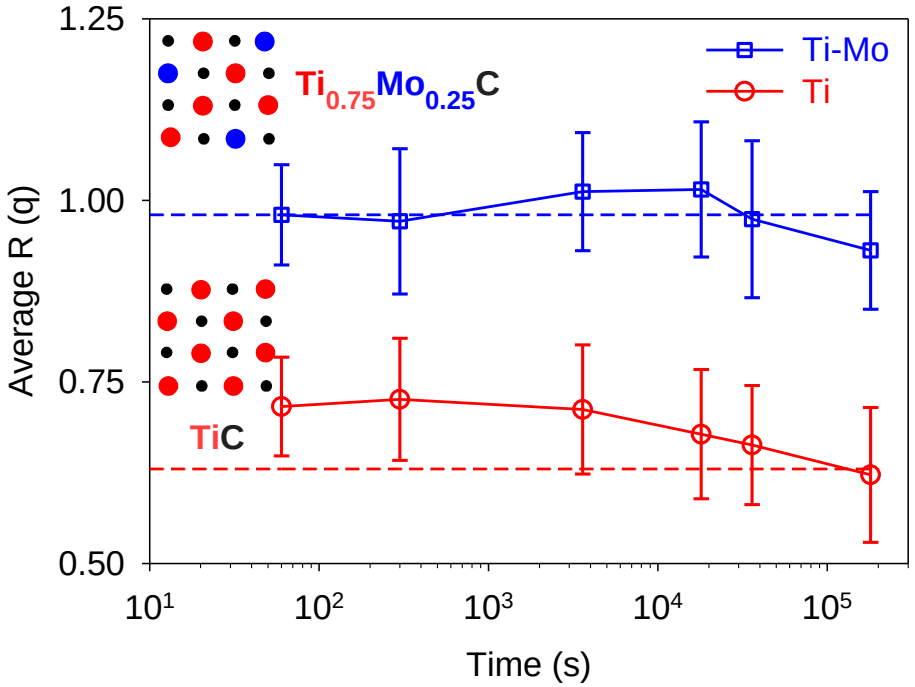

Fig. 3. Plot of the mean value of R(q) as a function of scattering vector, q, calculated from the scattering curves in Fig. 2. R(q) is the ratio of magnetic to nuclear scattering intensity. Theoretical values for TiC and for Ti0.75Mo0.25C are shown by the horizontal lines.

The volume percent (f_v) of TiC and (Ti, Mo)C were calculated from the invariant, Q, of the magnetic SANS signal using the equation $Q=\int_0^\infty I(q)q^2dq=2\pi^2\left(\rho_\rho-\rho_m\right)^2 f_v(1-f_v)$ [21, 24]. where ρ_p and ρ_m are the magnetic scattering length densities of precipitate and matrix. The

use of magnetic SANS signal ensures that the volume percent calculation is independent of the chemical composition of the precipitates. Fig. 4a shows that the volume percent of TiC in Ti steels and (Ti, Mo)C in TiMo steels were ~0.10% and ~0.13% respectively and invariant with isothermal holding. The equilibrium volume percent of 0.156 vol% (TiC phase fraction) and 0.157 vol% ((Ti, Mo)C phase fraction) at 650 °C calculated using Thermo-Calc and the TCFE7 database. In Ti-Mo steels, the atomic ratio of Ti to Mo in (Ti, Mo)C precipitates is about 9:1, which indicates the Mo is not thermodynamically preferred.

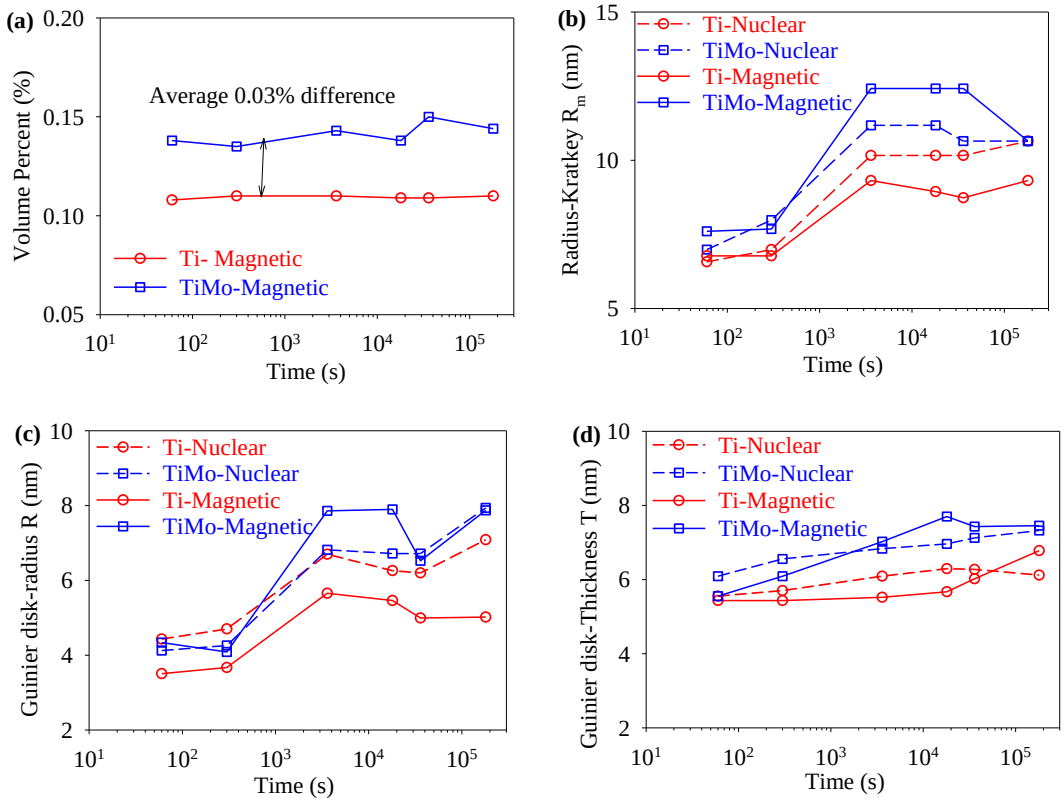

Fig. 4. Graphs to show the effect of isothermal holding time, t on carbide particle volume fraction and particle dimensions in Ti and TiMo alloys aged at 650 °C. (a) Particle volume percent calculated from analysis of the invariant, Q, of the magnetic SANS data. Particle dimensions obtained from (b) Kratky radius, R_{max}, assuming spherical-shaped particles and (c and d) Guinier analysis assuming disk-shaped particles. (c) shows the disk radius, R, versus ageing time, t, and (d) shows disk thickness, T, versus time, t.

Figs. 4b, 4c and 4d show the Kratky radius (R_{max}), Guinier radius (R) and thickness (T) (disk morphology [23]) of particles obtained from both nuclear and magnetic SANS scattering signs. The Kratky radius is calculated by $R_{max} = \sqrt{3}/q_{max}$ (the "pseudo-Guinier radius"), where the q_{max} determined from the the Kratky plot (Iq^2 vs q) [25]. Alternatively, a radius of gyration, R_{g1}, is extracted from the Guinier plot (which takes the form of ln(I) *vs* q^2) using a self-consistent method with $1<qR_{g1}<2$. Considering a distribution of monodisperse thin discs of thickness, T, and radius, R, the relationship between T, R and R_{g1} is given by

$R^2_{g1}=T^2/12+R^2/2$ [26]. A second Guinier plot of $\ln[q^2(I)]$ vs q^2 is known to give a radius of gyration, R_{g2}, that is related to the disc thickness, $R_{g2}=(T^2/12)^{0.5}$. Fig. 4b shows that the average size of the TiC and (Ti, Mo)C interphase precipitates increased from ~6.5nm after 60s to ~10nm after 3.6ks, but exhibit minimal growth during the further ageing up to 180ks at 650°C. The average Guiner radius (Fig. 4c) of disk precipitates has been found ~2nm smaller than Kratky radius, but followed very similar tendency as kratkey radius. Fig. 4d indicated that the average Gunier thicknesses of TiC and (Ti,Mo)C were ~5.5nm and ~6.5nm respectively and both exhibit insignificant evolution (<1.5nm) during isothermal ageing. Hence, the hypothesis that the Mo can retard the growth and coarsening of (Ti,Mo)C interphase precipitation is not dependable as the current results show the average precipitate size in aged Ti-containing steels were slightly smaller than in aged Ti-Mo-containing steels.

The precipitates coarsening rates in both alloys were extremely low. In Ti-containing steels it is known that a low Ti/C ratio (0.4) causes the concentration of Ti at the precipitate-ferrite interface to become small and therefore the diffusion gradients which drive coarsening become shallow and slow [11]. While in Ti-Mo added steels, although the Ti+Mo/C=1 and Mo incorporated into the precipitates at nucleation, the subsequent growth of precipitates is controlled by the diffusion of Ti atoms rather than Mo. We can conclude that the addition of Mo slightly improved the ageing-resistance of the steels (Fig. 1a) is due to (Ti,Mo)C having a reduced misfit strain between the carbide and ferrite matrix than TiC [8, 27], rather than Mo retarding coarsening of the precipitates. The (Ti,Mo)C carbides are more coherent and loose coherency at a larger size than TiC.

The addition of Mo also slightly increased the hardness of the steels (Fig. 1a). This is due to the higher volume percent of interphase precipitates rather than a decreased average size of precipitate. Approximately 25 at.% Mo co-precipitates as (Mo,Ti)C at the early stage of precipitation and this increased the volume percent of these precipitates from ~0.1% to ~0.13%. This yields ~7% improvement in the precipitation strengthening effect based on the Ashby-Orowan equation $\Delta\sigma_{ppt} = \frac{0.538Gbf_v^{0.5}}{2R} ln\left(\frac{R}{b}\right)$ [9, 28, 29]. Where, $\Delta\sigma_{ppt}$ is the increase in yield strength, G is the shear modulus, b is the Burgers vector, f_v is the carbide volume fraction and R is the mean carbide radius.

In summary, our SANS results (nuclear and magnetic scattering signals) reveal Mo does not play a role in retarding coarsening of the precipitates, which is contrary to existing literature. Instead, our results suggested that approximately 25 at.% Mo replaced Ti in the (Mo,Ti)C precipitates, both increasing the precipitate volume percent and average size, and changing the lattice spacing, altering the coherency which approved by high resolution TEM studies in [29]. The Ti-Mo steels have higher hardness and better ageing-resistance than Ti only steels is principally due to the decrease in misfit between the carbide and matrix leading to coherency being maintained to a larger carbide size in the case of the Ti-Mo alloyed steel. This new understanding opens opportunities for design of ageing-resistant microalloyed steels with significantly less amount of Mo.

References

[1] Y. Funakawa, T. Shiozaki, K. Tomita, T. Yamamoto, E. Maeda, ISIJ Int. 44(11) (2004) 1945-1951.

[2] A. Davenport, F. Berry, R. Honeycombe, Metal Sci. 2(1) (1968) 104-106.

[3] S.-P. Tsai, Y.-T. Tsai, Y.-W. Chen, J.-R. Yang, C.-Y. Chen, Y.-T. Wang, C.-Y. Huang, Scr. Mater. 143 (2018) 103-107.

[4] T. Gladman, Maney Pub1997.

[5] F. Yoshimsa, F. Takeshi, Y. Katsumi, JEF Tech. Rep. No. 18 (2013).

[6] Y. Funakawa, K. Seto, Tetsu-to-Hagane (Journal of the Iron and Steel Institute of Japan) 93(1) (2007) 49-56.

[7] C. Chen, H. Yen, F. Kao, W. Li, C. Huang, J. Yang, S. Wang, Mater. Sci. Eng. A. 499(1) (2009) 162-166.

[8] J.H. Jang, C.-H. Lee, Y.-U. Heo, D.-W. Suh, Acta Mater. 60(1) (2012) 208-217.

[9] N. Kamikawa, Y. Abe, G. Miyamoto, Y. Funakawa, T. Furuhara, ISIJ Int. 54(1) (2014) 212-221.

[10] Z. Wang, H. Zhang, C. Guo, W. Liu, Z. Yang, X. Sun, Z. Zhang, F. Jiang, J. Mater. Sci. 51(10) (2016) 4996-5007.

[11] J. Jang, C. Lee, H. Han, H. Bhadeshia, D. Suh, Mater. Sci. Technol. 29(9) (2013) 1074-1079.

[12] H.-W. Yen, P.-Y. Chen, C.-Y. Huang, J.-R. Yang, Acta Mater. 59(16) (2011) 6264-6274.

[13] H.-W. Yen, C.-Y. Huang, J.-R. Yang, Scripta Mater. 61(6) (2009) 616-619.

[14] Y.-J. Zhang, G. Miyamoto, K. Shinbo, T. Furuhara, Scr. Mater 69(1) (2013) 17-20.

[15] Y. Kobayashi, J. Takahashi, K. Kawakami, Scr. Mater. 67(10) (2012) 854-857.

[16] I. Timokhina, P. Hodgson, S. Ringer, R. Zheng, E. Pereloma, Scr. Mater. 56(7) (2007) 601-604.

[17] C. Enloe, K. Findley, C.M. Parish, M.K. Miller, B. De Cooman, J. Speer, Scr. Mater. 68(1) (2013) 55-58.

[18] J. Wang, M. Weyland, I. Bikmukhametov, M.K. Miller, P.D. Hodgson, I. Timokhina, Scr. Mater. 160 (2019) 53-57.

[19] R. Heenan, S. Rogers, D. Turner, A. Terry, J. Treadgold, S. King, Neutron News 22(2) (2011) 19-21.

[20] A. Michels, J. Weissmüller, Rep. Prog. Phys 71(6) (2008) 066501.

[21] Y. Wang, S. Clark, V. Janik, R. Heenan, D.A. Venero, K. Yan, D. McCartney, S. Sridhar, P. Lee, Acta Mater. 145 (2018) 84-96.

[22] B.S. Seong, E. Shin, S.-H. Choi, Y. Choi, Y.S. Han, K.H. Lee, Y. Tomota, Appl. Phys. A 99(3) (2010) 613-620.

[23] S. Mukherjee, I. Timokhina, C. Zhu, S. Ringer, P. Hodgson, Acta mater. 61(7) (2013) 2521-2530.

[24] F. De Geuser, A. Deschamps, C R Phys 13(3) (2012) 246-256.

[25] A. Deschamps, F. De Geuser, J. Appl. Crystallogr. 44(2) (2011) 343-352.

[26] T. Imae, T. Kanaya, M. Furusaka, N. Torikai, John Wiley & Sons2011.

[27] J. Jang, Y. Heo, C. Lee, H. Bhadeshia, D.-W. Suh, Mater. Sci. Technol. 29(3) (2013) 309-313.

[28] M.-Y. Chen, M. Gouné, M. Verdier, Y. Bréchet, J.-R. Yang, Acta Mater. 64 (2014) 78-92.
[29] P. Gong, X. Liu, A. Rijkenberg, W. Rainforth, Acta Mater. 161 (2018) 374-387.

Supplementary

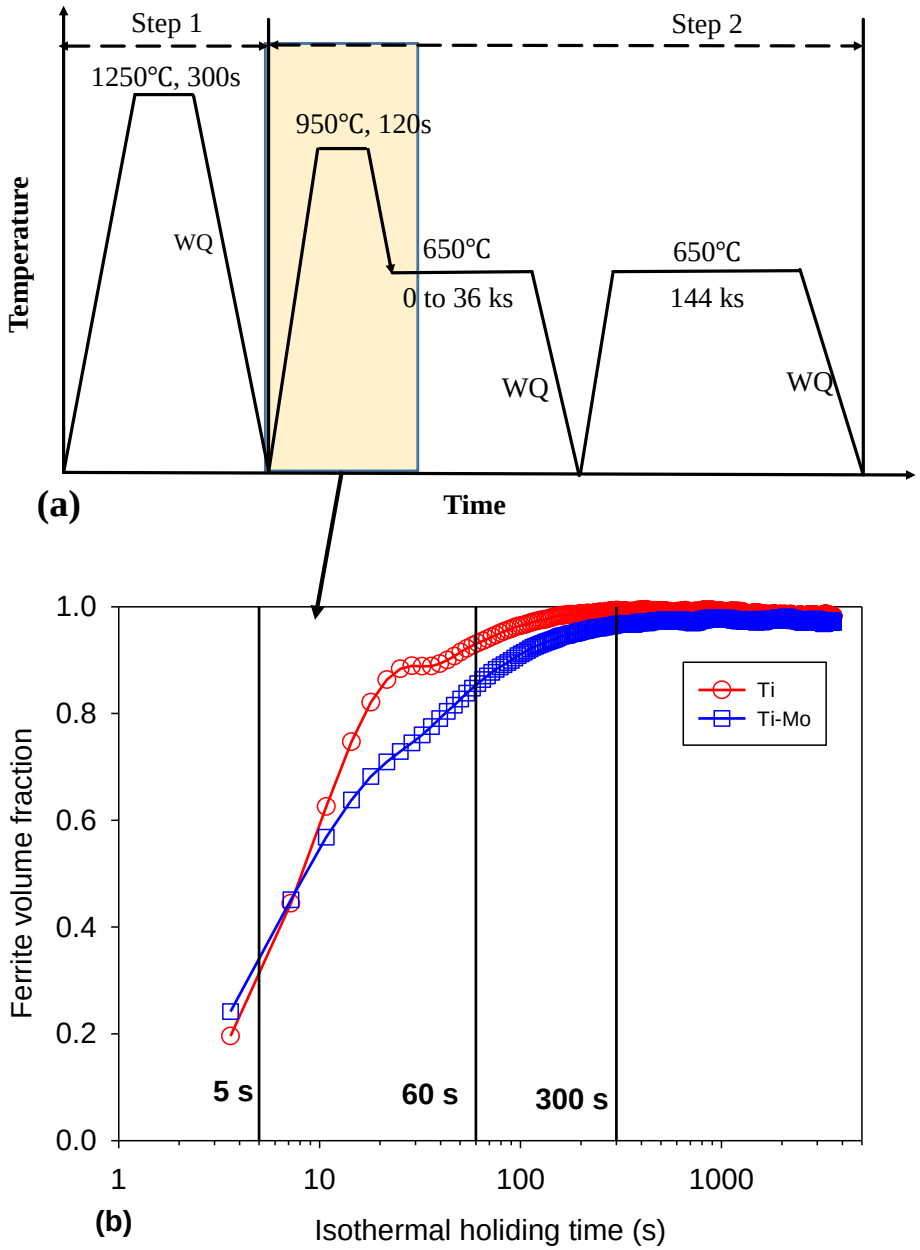

Fig. S1. (a) Schematic diagram showing the two-step heat treatment. The first heating temperature, 1250 °C, is determined to resolve (Ti, Mo)C precipitates and the second heating temperature and time are determined to control the austenite grain size. The ageing temperature is 650 °C. Prolonged 2400 min ageing time at 650 °C is designed to check the effect of the coarsening process and (b) variations in ferrite volume fraction with isothermal holding time (step 2) for Ti and Ti-Mo alloys at 650 °C.

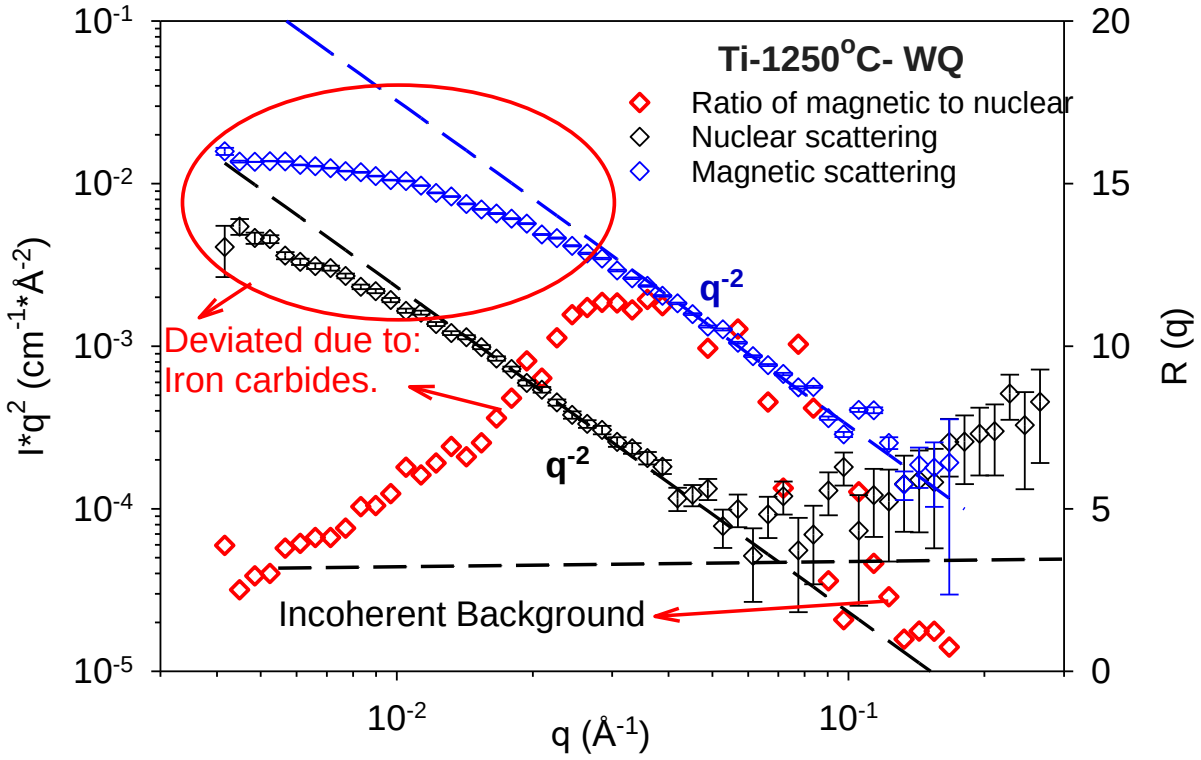

Fig. S2. One-dimensional nuclear and magnetic SANS patterns of Iq^2 and R(q) versus scattering vector, q, obtained from the Ti sample water quenched from 1250 °C. Labels indicate constituents that contribute significant scattering signals.

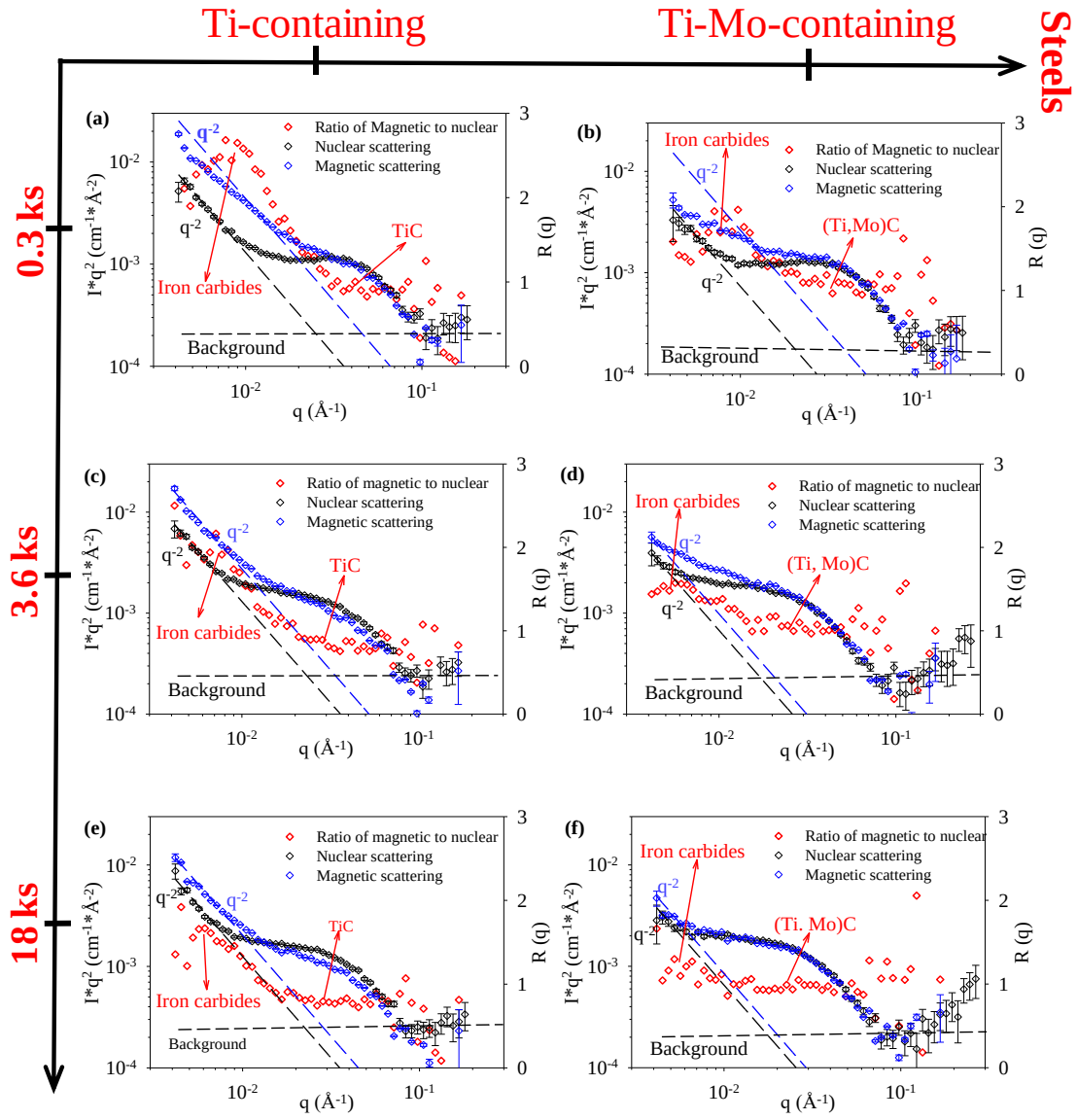

Fig. S3. One-dimensional nuclear and magnetic SANS patterns of Iq^2 (left hand axis) and R(q) (right hand) axis versus scattering vector, q, obtained from the Ti and TiMo alloy samples isothermally transformed at 650 °C for different times. (a), (c) and (e), Ti alloy for 0.3ks 3.6ks and 18ks respectively. (b), (d) and (f) TiMo alloy samples for for 0.3ks 3.6ks and 18ks respectively. Labels indicate constituents that contribute significant scattering signals.